Detection of subthreshold oscillations in a sinusoid-crossing sampling

Marisciel Litong and Caesar Saloma*
National Institute of Physics, University of the Philippines, Diliman 1101, Quezon City, The Philippines
(Received 12 June 1997; revised manuscript received 12 August 1997)

The detection threshold B of a sinusoid-crossing (SC) detector is improved using a new dithering technique. In a real SC detector, B is always greater than zero because the crossings could be located only with finite accuracy. Dithering is employed to determine the frequency f_s and the amplitude A_s of the subthreshold oscillation $s(t)=A_s\cos(2\pi f_s t)$, where $A_s<B$. The data representation of an analog input signal of bandlimit W, consists of locations $\{t_1,t_2,\ldots,t_{2M}\}=\{t_i\}$ where the signal intersects with the reference sinusoid $r(t)=A\cos(2\pi f_r t)$. A crossing exists within each interval $\Delta=1/2\,f_r=T/2M$, where T is the sampling period. If $W/2\leqslant f_r$, and the signal amplitude is less than A for all t values within T, then SC sampling satisfies the Nyquist sampling theorem. The unknown f_s value is determined from the power spectrum of the crossing locations of $[s(t)+n_\sigma(t)]$, where $n_\sigma(t)$ is the noise of variance σ^2. The A_s value is approximated from the signal-to-noise ratio (R) vs σ plot. The performance of the technique is studied from the R plots for different A_s, f_s, and T values. [S1063-651X(98)11402-2]

PACS number(s): 07.05.Hd, 06.20.−f, 06.30.−k, 07.07.−a

I. INTRODUCTION

A signal $s(t)$ of bandwidth W must be sampled at Nyquist rate and with an infinitely wide dynamic range so that it can be recovered without error from its sampled representation. Real sampling circuits, however, have finite detection limits because they are made from components with finite-time responses. The sampled representations of weak short-lived signals are therefore particularly prone to quantization errors.

There are two general methods of sampling a signal: (1) Amplitude sampling a t equal intervals Δ of time t, and (2) crossing or threshold sampling. In amplitude sampling, the sampled representation $\{s(i)\}$ of $s(t)$ within the sampling period $T=2M\Delta$, consists of equally spaced, quantized $s(t)$ values where $i=-M,\ -M+1,\ldots,M$. The Nyquist sampling criterion is satisfied if $s(t)$ is sampled at a rate $f_c=(1/\Delta)\geqslant W$.

In crossing sampling, $s(t)$ is sampled at unequal intervals of t, and its data representation consists of locations $\{t_i\}$ where $s(t)$ intersects a reference signal $r(t)$. Each t_i is a solution to $s(t)-r(t)=0$. The dc threshold sampling is the simplest form of crossing sampling that employs a constant reference signal. The utility of dc threshold sampling, however, is limited because for most types of input signals, it cannot satisfy the Nyquist sampling criterion.

Sinusoid-crossing (SC) sampling is a type of threshold sampling that utilizes a sinusoid reference signal: $r(t)=A\cos(2\pi f_r t)$. The Nyquist criterion is satisfied in SC sampling when (1) $A\geqslant|s(t)|$ for all t values within T, and (2) $f_r\geqslant W/2$. A crossing t_i exists within each interval $\Delta=1/2\,f_r=T/2M$, and the Fourier spectrum of $\{s(t_i)\}=\{r(t_i)\}$ can be computed directly from $\{t_i\}$ [1,2].

Because a crossing detector can be designed with only one comparator, it is considerably easier to build than the multicomparator analog-to-digital (AD) converter used in amplitude sampling [3,4]. Investigations regarding the performance of threshold-sampling schemes are also of considerable interest to biophysicists and neuroscientists because threshold sampling is the preferred mode of information coding in most biological neural networks [5–7].

In many cases, the detection threshold of the measuring instrument is held finite by quantization errors. In amplitude sampling with a q-bit AD converter, the detection threshold is $B=2A/2^q$, where $\pm A$ are the power supply voltages of the AD converter. Variations in the amplitude of $s(t)$ which are smaller than B are not recognized in the corresponding sampled representation. The sampling interval Δ is given by the conversion time of the AD converter.

The detection threshold of a real SC detector is also nonzero because it could locate a crossing position within $\Delta=1/2\,f_r$, only with finite accuracy due to the finite response times of its components [3,4]. In SC sampling, ac signals with peak-to-peak amplitude swings that are less than $2B$ are falsely detected as zero signals.

This paper demonstrates that dithering can be used to improve the effective detection threshold of a given SC detector. Dithering is a technique in digital signal processing that is used to minimize the effects of quantization errors [8,9]. It concerns the addition of noise $n_\sigma(t)$ of known variance σ^2, to the analog signal prior to its detection by the threshold detector.

Specifically, we show that dithering can be used to determine both the frequency f_s and amplitude A_s of the subthreshold oscillation $s(t)=A_s\cos(2\pi f_s t)$, where $A_s<B$. In the absence of dithering, $s(t)$ is erroneously detected by the SC detector as $s(t)=0$. The value is determined from the power spectrum $\{S_\sigma(f)\}$ that is produced from the crossing locations of $[s(t)+n_\sigma(t)]$ with $r(t)$.

The dithering technique is evaluated using benchmarks that are employed in the study of stochastic resonance [9,10] which is also about enhancing the detection of a subthreshold oscillation in a nonlinear system via the presence of noise.

We examine the quality of the power spectrum $\{S_\sigma(f)\}$

*Fax number: +632 9205474. Electronic address: csaloma@nip.upd.edu.ph

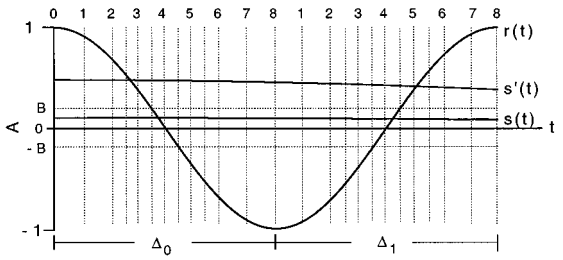

FIG. 1. Illustration of SC sampling where $r(t)=A\cos(2\pi f_r t)$. Same-frequency sinusoids $s(t)=A_s\cos(2\pi f_s t)$ and $s'(t)=A_s'\cos(2\pi f_s t)$ where $f_s<f_r$ intersect $r(t)$ at different locations since $A_s'\neq A_s$. The SC locations are established by dividing each $\Delta=1/2\,f_r$ into N partitions ($N=8$). Oscillation $s(t)$ is detected falsely as a zero signal because $A_s<B=A\pi/2N$.

as a function of σ, to determine the optimal conditions where dithering is most effective. We also establish how signal to noise ratio (R) of the spectral component at $f=f_s$ behaves as a function of σ for different values of f_s and A_s. The A_s value is approximated from the characteristics of the R vs σ plot. Both Gaussian noise (GN) and uniform white noise (UWN) are considered because they are the simplest types of noise to generate [11].

The presentation of our paper proceeds as follows. A brief discussion of the concept of detection limit in SC sampling is given in Sec. II. Section III outlines the dithering procedure that we have developed. Results of our numerical experiments are presented in Sec. IV. Various conditions are discussed in Sec. V, concerning the efficacy of the dithering technique.

II. SINUSOID-CROSSING SAMPLING

The SC representation of an analog input signal is characterized by two factors: (1) the order in which the various SC locations occur in the sequence $\{t_i\}$, and (2) the accuracy in which a crossing is located within each Δ.

Figure 1 illustrates how SC sampling works for two different sinusoids: $s(t)=A_s\cos(2\pi f_s t)$, and $s'(t)=A_s'\cos(2\pi f_s t)$ where $r(t)=A\cos(2\pi f_r t)$, $A\geqslant A_s'>B>A_s$, and $f_r=(1/2\Delta)>f_s$. The data representations of $s(t)$ and $s'(t)$ are given by the crossing locations $\{t_i\}$ and $\{t_i'\}$, which are solutions to $s(t)=r(t)$ and $s'(t)=r(t)$, respectively.

In practice [3,4], the location of a SC within the interval Δ is established by subdividing Δ into N partitions (in Fig. 1, $N=8$). All the $2M$ SC's that occur within T have to be located as accurately as possible to minimize the effects of quantization errors which are manifested as spurious frequency components in the computed Fourier spectrum [12].

The SC location in the ith interval Δ_i is given by $t_i=\Delta[(i-1)+p_i/N]$, where p_i is the particular partition within Δ_i where $s(t)=r(t)$. Note that the SC's of a zero input signal are all found at $p_0=p_1=\cdots=p_{2M-1}=N/2$. In Fig. 1, for example, the first two SC's of $s(t)$ are at $p_0=\frac{4}{8}$, and $p_1=\frac{4}{8}$, respectively, because $A_s<B$. For $s'(t)$ on the other hand, the SC's are found at $p_0'=\frac{3}{8}$, $p_1'=\frac{5}{8}$. Because $s(t)$ and $s'(t)$ have different amplitudes, $\{p_i\}\neq\{p_1'\}$.

On the other hand, two sinusoids of the same amplitude ($A_s''=A_s$) but different frequencies ($f_s\neq f_s'$) also have different p_i sequences. A barely detectable signal ($A_s\approx$detection limit B) has SC's that can only be at $p_i=(N-2)/2$, $N/2$, or $(N+2)/2$. The number of possible p_i values where the SC's could occur increases with the amplitude of $s(t)$.

The accuracy of locating a SC improves with the number of partitions N made within Δ. Real SC detectors could locate the position of a SC only with finite accuracy because the smallest partition ($\Delta/2N$) that is possible within Δ can never be made less than the response time δ of the detection circuit [3,4]. Finite detection accuracy results in a finite value of the detection threshold B where $B=(\frac{1}{2})|\delta r(t=p_i\Delta/N=\Delta/2)|(\frac{1}{2})|2\pi f_r A\sin[2\pi f_r(t=\Delta/2)]\delta t|=\pi A/2N$, where $\delta t=\Delta/N$ and $f_r=1/2\Delta$. For a given reference amplitude A, B approaches zero as N approaches infinity.

The quantization error E associated with a real SC detector is given by

$$E=E(t)=(1/2)|\delta r(t)|=(\pi f_r\delta t A)|\sin(\pi p_i/N)|$$
$$=(\pi A/N)|\sin(\pi p_i/N)|=B|\sin(\pi p_i/N)|.$$

The amplitude representation $x(p_i)$ of the analog input signal $x(t)$ within the interval Δ_i is given by $x(p_i)=r(p_i\Delta/N)\pm B|\sin(\pi p_i/N)|$. The error in $x(p_i)$ is therefore smallest for values of $x(t)$ which are comparable to A and is largest for small $x(t)$ values whose SC's occur near $p_i=N/2$.

We have previously established that a SC-based AD conversion performs like an 8-bit conventional AD converter when $N=2^{11}$ [1]. The SC's of $s(t)$ are all found at $\{t_i\}=\{\Delta[(i-1)+\frac{1}{2}]\}$ because $A_s<B=A\pi/2N$. Thus $s(t)$ is erroneously detected as a zero signal.

III. DITHERING AND DETECTION OF WEAK OSCILLATIONS IN SC SAMPLING

Illustrated in Fig. 2 is the flowchart of the dithering procedure that we have developed to determine the unknown f_s and A_s values of the subthreshold oscillation $s(t)=A_s\cos(2\pi f_s t)$, where $A_s<B$. The analog inputs to the SC detector are the reference $r(t)$ and $[s(t)+n_\sigma(t)]$. The output of the comparator changes state (state 1 or 0) every time: $s(t)+n_\sigma(t)=r(t)$. The SC detector locates a crossing only once within each interval Δ.

For a given σ value, we obtain ten independent SC representations of $[s(t)+n_\sigma(t)]$. Using ten uncorrelated $n_\sigma(t)$ sequences. From the ten data representations $\{t_i\}_1$, $\{t_i\}_2,\ldots,\{t_i\}_{10}$ the most probable t_i value $\langle t_i\rangle$ is derived for each of the $2M$ Δ_i's within T. In practice, the $\{t_i\}$'s may be obtained by having ten SC detectors sample $s(t)$ simultaneously. The detectors utilize one common $r(t)$ signal but each uses its own uncorrelated noise source $n_\sigma(t)$.

Because $s(t_i)+n_\sigma(t_i)=r(t_i)$, the data set $\{r(\langle t_i\rangle)\}$ provides an unequally sampled amplitude representation of $s(t)+n_\sigma(t)$, where $\langle t_i\rangle$ is the average t_i value. From $\{r(\langle t_i\rangle)\}$, we generate an equally sampled representation $\{[s(iT/2M)+n_\sigma(iT/2M)]\}$ by cubic-spline interpolation [13]. Finally, the discrete power spectrum $\{S_\sigma(f)\}=\{S_\sigma(f=k/T)\}$ is computed by Fourier transforming the autocorrelation $\gamma_\sigma(iT/2M)$ of $\{[s(iT/2M)+n_\sigma(iT/2M)]\}$ where $k=-M,\,-M+1,\ldots,M$.

It must be noted that the two signals $s(t)=A_s\cos(2\pi f_s t)$ and $s''(t)=A_s\cos(2\pi f_s t+\phi)$ where ϕ is the

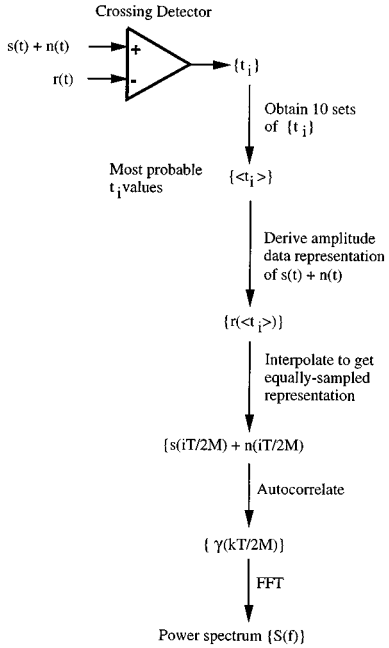

FIG. 2. Flowchart of the procedure used to compute the power spectrum $S_\sigma(f)$ of the dithered signal: $s(t)+n_\sigma(t)$, where $s(t)=A_s\cos(2\pi f_s t)$ and $A_s<B$. At the proper noise variance σ^2, $\{S_\sigma(f)\}$ will contain only one prominent line that is found at $f=f_s$.

phase, have identical power spectra, and could not be discerned from each other. This is because $\{S_\sigma(f)\}$ is computed from the autocorrelation of a data representation containing the relative locations of the SC crossings.

IV. NUMERICAL EXPERIMENTS

We perform a number of numerical experiments to determine the efficacy of dithering in SC sampling. The procedure outlined in Fig. 2 was employed to compute the power spectrum $\{S_\sigma(f)\}$ of $s(t)+n_\sigma(t)$, where $s(t)=A_s\cos(2\pi f_s t)$ and $A_s<B$. The noise sequences were generated following the procedure found in Refs. [1, 14]. All computations were done using a DEC Alphaserver (Digital Equipment Corp. Model 2000-4/275).

A. Information contained in the power spectrum

Figure 3(a) shows the power spectrum $\{S_\sigma(f)\}$ obtained when $s(t)=0.192B\cos(2\pi 16t)$ is dithered with UWN at $\sigma=0.018$, where $r(t)=2.5\cos(2\pi 512t)$, $B=0.015\,339\,8$, $T=1$, $f_s=16=0.031\,25f_r$, $N=2^8=256$, and $2M=1024$. Note that when $n_\sigma(t)=0$, the SC's of $s(t)$ are all found at $p_0=p_1=\cdots=p_{1023}=N/2=128$; and the corresponding $\{S_\sigma(f)\}=0$.

The spectrum exhibits only one prominent line at $f=f_s=16$ that is riding over a broadband-noise background. The component $S_\sigma(f_s=16)$ has a value of 45.98 and no other spectral component in $\{S_\sigma(f)\}$ has a magnitude that is greater than unity. The unknown f_s value can therefore be determined without ambiguity, from $\{S_\sigma(f)\}$.

The 1024 $\langle t_i\rangle$ values used to compute $\{S_\sigma(f)\}$ were obtained in the following manner: (1) Calculate the average p_i value: $p_i^{(a)}=(1/10)[n_1+2n_2+\cdots+127n_{127}+128n_{128}+129n_{129}+\cdots+256n_{256}]$ from $\{t_i\}_1$, $\{t_i\}_2,\ldots,\{t_i\}_{10}$, where n_{127} is the number of times (out of ten) that the SC occurs at $p_i=127$ (a similar definition holds for n_{128}, n_{129}, etc.); (2) truncate p_{i-a} to its greatest integer value $\langle p_i\rangle$ (e.g., if $p_i^{(a)}=127.9$, then $\langle p_i\rangle=127$, or if $p_i^{(a)}=128.8$ then $\langle p_i\rangle=128$, etc.); (3) calculate the average t_i value: $\langle t_i\rangle=[(i-1)\Delta/N+\langle p_i\rangle/N]=[(i-1)+\langle p_i\rangle/256]$; (4) repeat steps (1)–(3) for each of the $2M=1024\Delta$'s. The equally sampled representation $\{[s(iT/2M)+n_\sigma(iT/2M)]\}$ is interpolated from $\{r(\langle t_i\rangle)\}$.

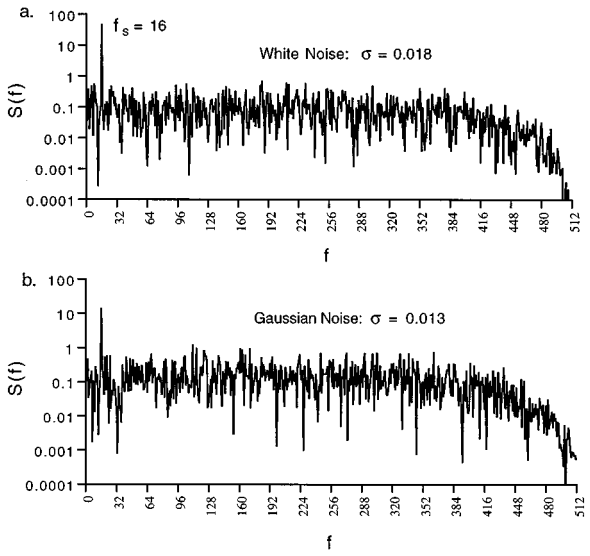

FIG. 3. Power spectrum $S_\sigma(f)$ of $s(t)=0.192B\cos(2\pi 16t)$ when dithered with uniform white noise of $\sigma=0.018$ and Gaussian noise of $\sigma=0.013$, where $r(t)=2.5\cos(2\pi 512t)$, $B=0.015\,339\,8$, $T=1$, $2M=1024$, and $N=256$. In the absence of dithering, $s(t)$ is detected falsely as a zero signal.

At the appropriate noise variance, longer segments in the sequence $\{[s(iT/2M)+n_\sigma(iT/2M)]\}$ will exhibit the periodicity of $s(t)$ as their fundamental period. The occurrence of the periodicity is highlighted more clearly in the autocorrelation $\gamma_\sigma(kT/2M)$ of $\{[s(iT/2M)+n_\sigma(iT/2M)]\}$ [13]. The frequency f_s of $s(t)$ is determined from the power spectrum $\{S_\sigma(f)\}$ which is the Fourier transform of $\gamma_\sigma(kT/2M)$. The value of $S_\sigma(f=f_s)$ increases with the total length of the segments in the sequence $\{[s(iT/2M)+n_\sigma(iT/2M)]\}$, that exhibits the periodicity of $s(t)$.

Shown in Fig. 3(b) is the computed $\{S_\sigma(f)\}$ that was obtained when $s(t)$ is dithered with Gaussian noise where $\sigma=0.013$. Note that $S_\sigma(f_s=16)$ is the only prominent line in $\{S_\sigma(f)\}$. The unknown f_s value can therefore be determined without ambiguity, from $\{S_\sigma(f)\}$.

B. Amplitude of subthreshold oscillation

The dithering technique is evaluated as a function of amplitude A_s of $s(t)=A_s\cos(2\pi 16t)$ where $A_s<B$. The choice of $f_s=16$ is purely arbitrary. Presented in Figs. 4(a)–4(c) are R vs σ plots where $R=[S_\sigma(f_s)-N_\sigma(f_s)]/[N_\sigma(f_s)]$, and $N_\sigma(f_s)$ is the value of the noise spectrum $\{N_\sigma(f)\}$ at $f=f_s$.

The $N_\sigma(f_s)$ value is determined from the best-fit curve of the data set $\{S_\sigma^b(f)\}=\{S_\sigma(1),\ldots,S_\sigma(f_s-1)\}$, blank, $S_\sigma(f_s+1),\ldots,S_\sigma(2M-1)\}$, which represents the noise back-

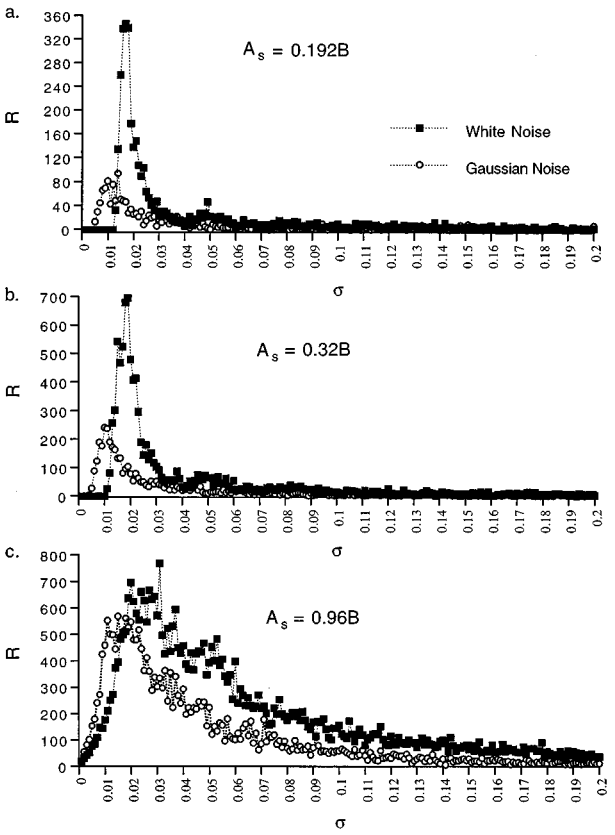

FIG. 4. R vs σ plots obtained when $s(t)=A_s\cos(2\pi 16t)$ is dithered with Gaussian noise (circles) and uniform white noise (squares), respectively: (a) $A_s=0.192B$, (b) $A_s=0.32B$, and (c) $A_s=0.96B$, where $r(t)=2.5\cos(2\pi 512t)$, where $B=0.015\,339\,8$, $T=1$, $2M=1024$, and $N=256$.

ground in $S_\sigma(f)$. A least-squares error curve-fitting procedure [15] is used to determine the third-order polynomial curve $S^c_\sigma(f)$ that fits best the noise background $\{S^b_\sigma(f)\}$. The $N_\sigma(f_s)$ value is given by $N_\sigma(f_s)=S^c_\sigma(f=f_s)$.

The R vs σ plots in Fig. 4(a) correspond to the case of $A_s=0.192B$, where $B=0.015\,339\,8$, $r(t)=2.5\cos(2\pi 512t)$, $T=1$, $f_s=16=0.031\,25f_r$, $N=2^8=256$, and $2M=1024$. Note that $|B-A_s|\approx 0.0124$. For both types of noise, the R_σ does not decrease monotonically with σ.

With GN dithering, the onset of the nonlinear behavior of the R vs σ plot occurs at $\sigma\approx 0.005$. With UWN dithering, the onset happens at a stronger noise strength of $\sigma\approx 0.013$. Once the onset is achieved, the R increases rapidly until the peak R value is achieved. The R vs σ plot peaks at $\sigma=\sigma_w\approx 0.017$, with UWN dithering, while with GN it peaks at $\sigma=\sigma_g\approx 0.014<\sigma_w$, with GN dithering. The corresponding $\{S_\sigma(f)\}$'s of the R values produced at $\sigma=\sigma_w$ and $\sigma=\sigma_g$ are the ones shown in Figs. 3(a) and 3(b), respectively.

The two R vs σ plots in Fig. 4(a) have different characteristics because UWN and GN are described by different probability distribution functions [11]. For UWN, the possible amplitude values lie with equal probability within the range $-\sigma<n_\sigma(t)<+\sigma$ (box-type distribution). On the other hand, amplitude values which are greater than $|\sigma|$ are still possible for a GN sequence of a given σ value because a Gaussian probability distribution function does not immediately go to zero beyond $\pm\sigma$. This property is the reason why the onset of the nonlinearity of the R vs σ plot occurs at a lower σ value with GN dithering.

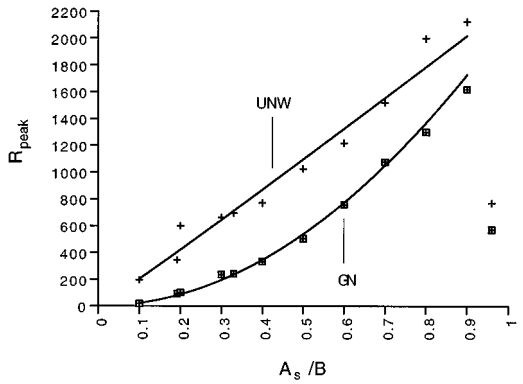

FIG. 5. R_{peak} vs A_s plot obtained when $s(t)=A_s\cos(2\pi 16t)$ is dithered with uniform white noise (cross) and Gaussian noise (square), where $r(t)=2.5\cos(2\pi 512t)$, $B=0.015\,339\,8$, $T=1$, $2M=1024$, and $N=256$.

The peak value R_{peak} that is obtained at $\sigma=\sigma_w$ is roughly 3.7 times stronger than what is produced by GN dithering at $\sigma=\sigma_g$. This indicates that UWN dithering is more effective in determining the periodicity of $s(t)$.

At $A_s\approx 0.32B$ or $|B-A_s|\approx 0.0104$, an increase in the R_{peak} value is obtained for both noise types [see Fig. 4(b)]. The peak values occur at $\sigma_g=0.010$ and $\sigma_w=0.019$, respectively. The R_{peak} obtained with UWN dithering is 2.9 times stronger than the one produced using GN dithering.

Figure 4(c) ($A_s=0.014\,726\approx 0.96B$, $|B-A_s|\approx 0.006$) illustrates that the R plot broadens with increasing A_s. The R_{peak} values are found at $\sigma_w=0.031$ and $\sigma_g=0.015$, respectively. The difference in their peak values decreases with increasing A_s value. At $A_s\approx 0.96B$, the onset of the nonlinear behavior of the R vs σ plots occurs almost immediately at $\sigma=0.001$.

The R plots obtained using UWN dithering [Figs. 4(a)–4(c)] also exhibit another weaker hump around $\sigma\approx 0.053$. This behavior reflects the multithreshold behavior of SC sampling. The separation between two successive threshold levels centered at $r(p_i)$ is given by $|\delta r(p_i)|=(\pi f_r/N)|A\sin(\pi p_i/N)|$. The level separations are nonuniform and are decreasing with increasing $r(t)$.

Figure 5 shows the dependence of the R_{peak} value on A_s. Within the range $0.1B\leqslant A_s\leqslant 0.9B$, a single-valued dependence exists between R_{peak} and A_s which indicates that our dithering technique is capable of discriminating one A_s value from another. Assuming a power-law dependence, the best-fit curve corresponding to the data points obtained using UWN dithering is given by $R_{\text{peak}}=2255.64A_s^{1.040}$, where $0.1B\leqslant A_s\leqslant 0.9B$. For the data points that were obtained using GN dithering the best-fit curve is $R_{\text{peak}}=2133.07A_s^{1.983}$.

The R_{peak} does not continue to increase with A_s beyond $A_s=0.9B$. For $A_s=0.9B$, the values have decreased to $R_{\text{peak}}\approx 768$ for UWN dithering, and $R_{\text{peak}}\approx 569$ for GN dithering. The corresponding R vs σ plots for $A_s=0.9B$ are shown in Fig. 4(c).

Low R values are associated with $\{S_\sigma(f)\}$'s that exhibit many other prominent spectral lines aside from the one at $f=f_s=16$. The correct f_s value is therefore difficult to recog-

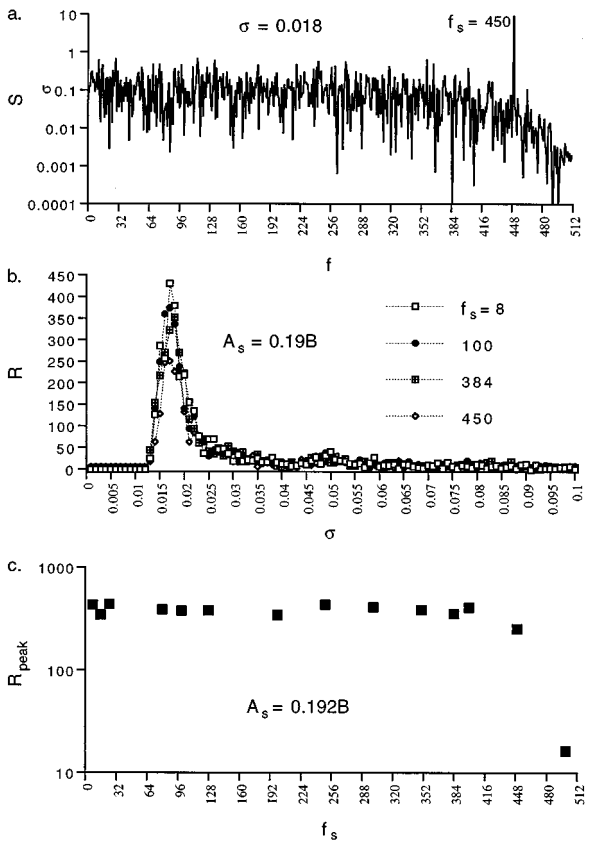

FIG. 6. Uniform white-noise dithering of $s(t)=0.002\,91\cos(2\pi f_s t)$: (a) $S_\sigma(f)$ corresponding to $f_s=450$ at $\sigma=0.018$, (b) R plots for $f_s=8$, 80, 384, 450; and (c) R_{peak} vs f_s plots, where $r(t)=2.5\cos(2\pi 512t)$, where $B=0.015\,339\,8$, $T=1$, $2M=1024$, and $N=256$.

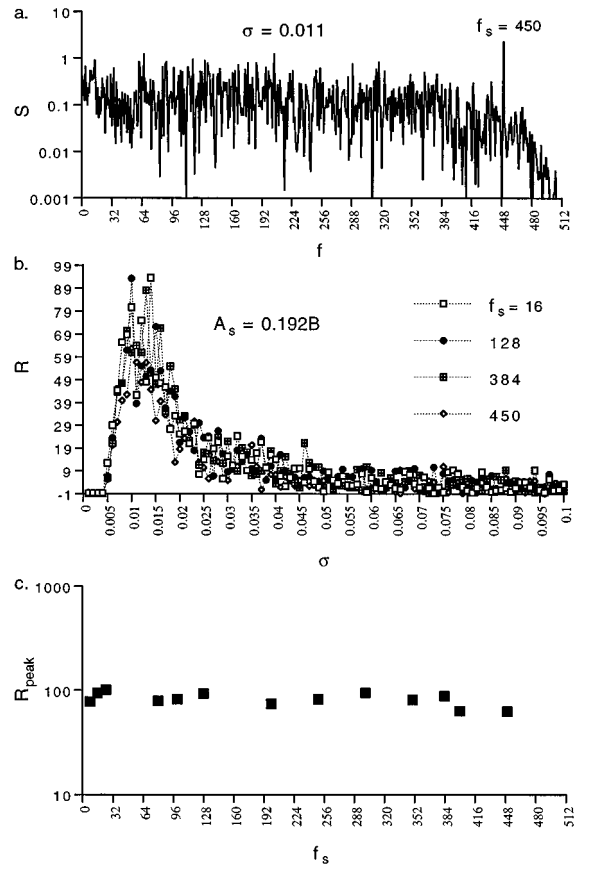

FIG. 7. Gaussian-noise dithering of $s(t)=0.002\,91\cos(2\pi f_s t)$: (a) $S_\sigma(f)$ for $f_s=450$ and $\sigma=0.011$, (b) R plots for $f_s=8$, 80, 384, 450; and (c) R_{peak} vs f_s plot. Parameters: $r(t)=2.5\cos(2\pi 512t)$, $B=0.015\,339\,8$, $T=1$, $2M=1024$, and $N=256$.

nize from such kinds of spectra.

C. Frequency of subthreshold oscillation

We examine how the R_{peak} changes as a function of f_s when the oscillation amplitude A_s is held constant.

In Fig. 6(a) is the $\{S_\sigma(f)\}$ plot obtained when $s(t)=0.192B\cos(2\pi f_s t)=0.0029\cos(2\pi f_s t)$ is dithered with UWN at $\sigma=0.018$, where $r(t)=2.5\cos(2\pi 512t)$, $T=1$, $N=256$, $B=0.015\,339\,8$, and $2M=1024$. $f_s=450\approx 0.88 f_r$, $2M=1024$, $N=256$, and $B=0.015\,339\,8$. The power spectrum features only one prominent line which is found at $f=f_s=450$.

Shown in Fig. 6(b) are the R vs σ plots for different f_s values (UWN dithering). Note that the R value always peaks within the narrow range $0.016\leqslant\sigma_w\leqslant 0.018$, regardless of the f_s value. This behavior indicates that the mechanism behind the nonlinear behavior of R with σ is not in the strictest sense stochastic resonance [9].

Figure 6(c) illustrates the dependence of R_{peak} with f_s. Within the range $f_s\leqslant 400\approx 0.78 f_r$, the $R_{\text{peak}}(f_s)$ values have a standard deviation that is about 8.67% of the mean value. Relative to the mean $R_{\text{peak}}(f_s)$ value within the range $f_s\leqslant 0.78 f_r$, the -3 dB value of the f_s response is slightly less than $f_s=450=0.89 f_r$. An ideal frequency response corresponds to zero standard deviation.

The $\{S_\sigma(f)\}$ corresponding to $f_s=450$ still has only one prominent line at $f_s=450$. At $f_s=500$, however, other strong lines are already present in the corresponding $\{S_\sigma(f)\}$ and the correct f_s value can no longer be determined with certainty.

We also investigated the performance of the dithering technique when GN is used. Figure 7(a) presents the $\{S_\sigma(f)\}$ that is obtained when $s(t)=0.192B\cos(2\pi 450t)$ is dithered with GN at $\sigma=0.011$, where $r(t)=2.5\cos(2\pi 512t)$, $T=1$, $f_s=16=0.031\,25 f_r$, $N=2^8=256$, $B=0.015\,339\,8$, and $2M=1024$. The power spectrum has only one prominent line, and it is found at $f=f_s=450$.

Shown in Fig. 7(b) are the R vs σ plots for different f_s values (GN dithering). The SNR_σ plots peak within the narrow range $0.008\leqslant\sigma_w\leqslant 0.014$, independent of the f_s value which indicates that the nonlinear behavior of R with σ is not, in the strictest sense, stochastic resonance.

Figure 7(c) illustrates the dependence of R_{peak} with f_s when GN dithering is used. Within the range $f_s\leqslant 384\approx 0.75 f_r$, the $R_{\text{peak}}(f_s)$ values have a standard deviation of about 9.7% of their mean value. The ideal frequency response corresponds to zero standard deviation. Relative to the mean $R_{\text{peak}}(f_s)$ value within the range $f_s\leqslant 0.75 f_r$, the -3 dB value of the f_s response is near $f_s=450=0.89 f_r$.

The associated $S_\sigma(f)$ corresponding to $f_s=450$ still has only one prominent line at $f_s=450$. At $f_s=500$, however, strong lines other than at $f\neq f_s$ are already present in $S_\sigma(f)$

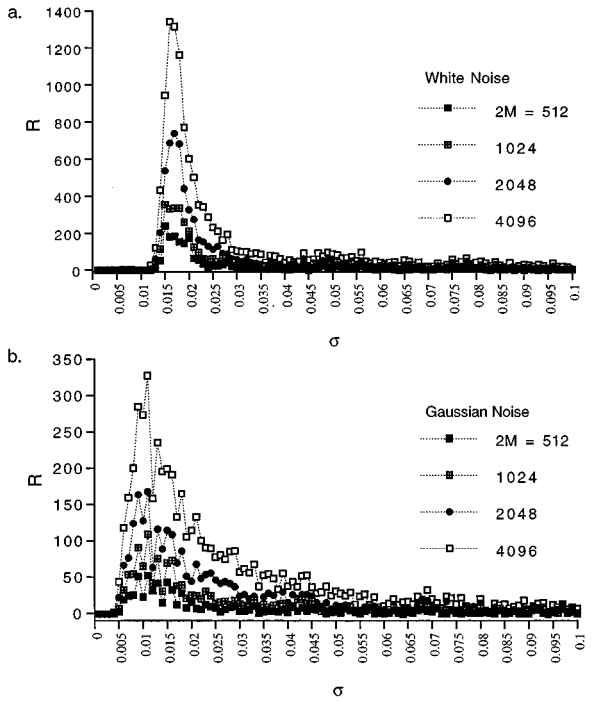

FIG. 8. R vs σ plots for $2M=512$, 1024, 2048, and 4096. Signal $s(t)=0.19B\cos(2\pi 16t)$ is dithered with (a) Uniform white noise, and (b) Gaussian noise, where $r(t)=2.5\cos(2\pi 512t)$, $A=2.5$, $T=2M\Delta=1$, $f_r=1/2\Delta=512$, $N=256$, and $B=0.015\,339\,8$.

and the correct f_s value can no longer be determined with certainty.

The $SNR_\sigma(f)$ plots presented in Figs. 6 and 7 show that better performance is obtained when $s(t)$ is dithered with UWN.

D. Sampling period T

We also examine how the length of $T=2M\Delta$ affects the performance of the dithering technique. This issue is relevant in the observation of subthreshold oscillations which are short lived and the possible T values are limited by the signal lifetime. In the numerical experiments, the SC sampling is always done at a constant sampling rate of $2f_r=1/\Delta=1024$.

Figure 8(a) shows the R plots obtained for $2M=512$, 1024, 2048, and 4096. The oscillation $s(t)=0.192B\cos(2\pi 16t)$ is dithered with UWN where $r(t)=2.5\cos(2\pi 512t)$, $T=1$, $N=256$, $B=0.015\,339\,8$, and $2M=1024$. The R plots always peak near $\sigma=\sigma_w\approx 0.017$, and their peak values increase linearly with M according to (best-fit curve) $R_{\text{peak}}=0.626M+67.5$.

Figure 8(b) shows R plots in the case when $s(t)$ is dithered with GN. The plots all peak near $\sigma=\sigma_g\approx 0.011$. The R_{peak} value also increases linearly with M according to (best-fit curve) $R_{\text{peak}}=0.15M+20.56$.

The results presented in Figs. 8(a) and 8(b) indicate that a long-lived oscillation is easier to detect than a short-lived one. Longer sampling periods also permit spectral analysis at a higher frequency resolution because $\delta f=1/T=1/2M\Delta$. Note, however, that the computational complexity of $\gamma(kT/2M)$ is $(2M)^2$, and therefore the calculation of $\{S(f)\}$ for long t_i sequences also takes much longer.

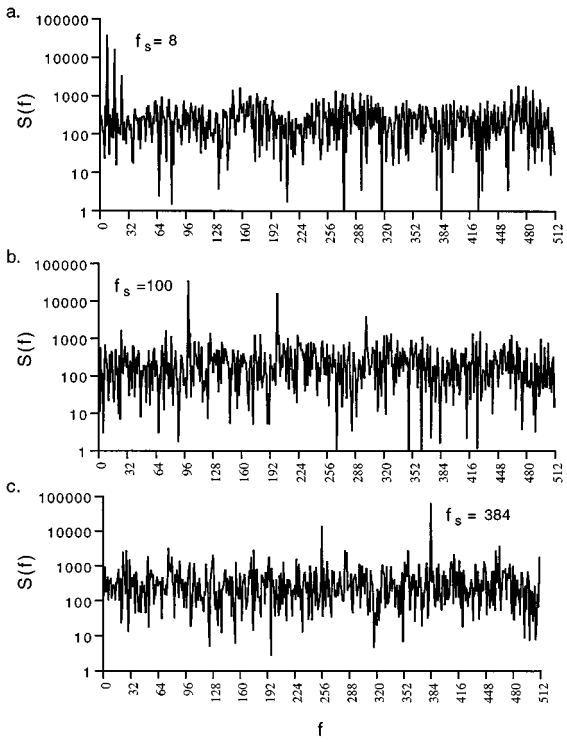

FIG. 9. dc threshold sampling. Power spectrum obtained when $s(t)=0.002\,91\cos(2\pi f_s t)$ is dithered with Gaussian noise: (a) $f_s=8$ ($\sigma=0.001$), (b) $f_s=100$ ($\sigma=0.001$), and (c) $f_s=450$ ($\sigma=0.001$). Only one dc crossing can possibly occur within each Δ ($\pm B=\pm 0.015\,339\,8$, $T=1024\Delta$, $\Delta=\frac{1}{512}$).

E. Dithering in dc threshold sampling

We compare our previous results with the case where $0.192B\cos(2\pi 16t)+n_\sigma(t)$ is sampled with respect to two symmetrical dc thresholds at $r(t)=\pm B=\pm 0.015\,339\,8$ [9]. At most, only one dc crossing $t_i^{(\text{dc})}$ can occur within each $\Delta=\frac{1}{1024}$ and a maximum of $2M$ dc crossings can be observed within a given T. In the absence of dithering, no intersections are possible between any of the two dc thresholds and $s(t)=0.192B\cos(2\pi 16t)\approx 0.0029\cos(2\pi 16t)$.

First, we determine the dc crossing locations of $[0.0029\cos(2\pi 16t)+n_\sigma(t)]$ with $r(t)=\pm 0.015\,339\,8$. A train of pulses $p(t)$ is derived from the locations of the dc crossings, according to the following rule: $p(t)=0$ when $|0.0029\cos(2\pi 16t)+n_\sigma(t)|<B$; $p(t)=1$ when $[0.0029\cos(2\pi 16t)+n_\sigma(t)]>0.015\,339\,8$; and $p(t)=-1$ when $[0.0029\cos(2\pi 16t)+n_\sigma(t)]<-0.015\,339\,8$. The power spectrum $\{S_\sigma(f)\}$ is then computed by Fourier transforming the autocorrelation of $p(t)$.

Presented in Figs. 9(a)–9(c) are the computed $\{S_\sigma(f)\}$'s corresponding to $f_s=8$, 100, and 450, respectively ($T=1024\Delta$, $\Delta=\frac{1}{1024}$, and $B=0.015\,339\,8$). The undetectable oscillation $s(t)=0.0029\cos(2\pi 16t)$ is dithered with GN at σ's that yield the maximum SNR_σ value of the $S(f=f_s)$ line. Each $\{S_\sigma(f)\}$ represents an average over ten raw power spectra.

To determine the dc crossing within a given Δ, the dithered signal $[0.0029\cos(2\pi 16t)+n_\sigma(t)]$ is compared 256 times (Δ is subdivided into 256 partitions) with the value of $r(t)$ for a possible intersection.

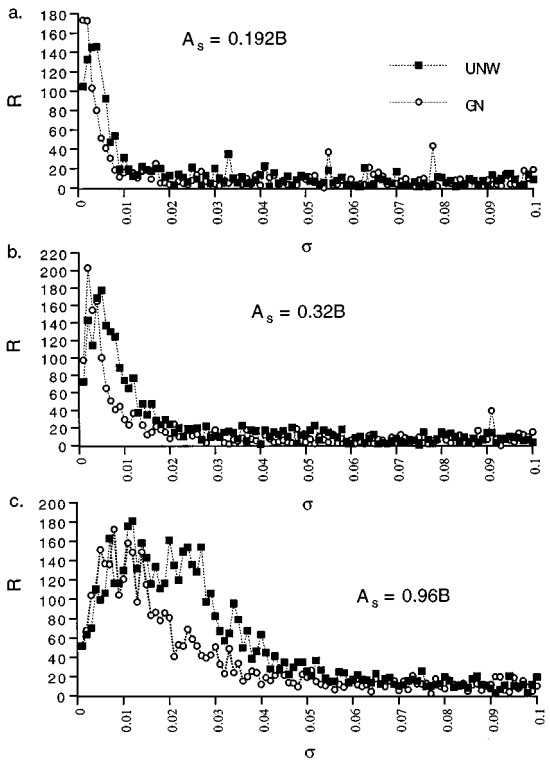

FIG. 10. dc threshold sampling ($\pm B=\pm 0.015\,339\,8$, $T=1024\Delta$, $\Delta=\frac{1}{512}$). R plots obtained when $s(t)=A_s\cos(2\pi 16t)$ is dithered with Gaussian (circle) and uniform white noise (square), respectively: (a) $A_s=0.19B$, (b) $A_s=0.32B$, and (c) $A_s=0.96B$.

Although the strongest $S_\sigma(f)$ component always occurs at $f=f_s$, it is not the only prominent line in $\{S_\sigma(f)\}$. The appearance of unwanted lines makes the determination of the correct f_s value quite difficult.

Presented in Figs. 10(a)–10(c) are R plots for different A_s values of $s(t)=A_s\cos(2\pi 16t)$, where $R=[S_\sigma(f_s)-N_\sigma(f_s)]/N_\sigma(f_s)$, and $f_s=16$. The $N_\sigma(f_s)$ value is determined from the curve fit $S^c_\sigma(f)$ of the sequence $\{S^b_\sigma(f)\}=\{\text{blank}, S_\sigma(1),\ldots,S_\sigma(f_s-1),\text{blank}, S_\sigma(f_s+1),\ldots,S_\sigma(2M-1)\}$, which represents the noise background in $\{S_\sigma(f)\}$. Other peaks were also removed from $\{S^b_\sigma(n)\}$ when their magnitudes are within two orders of magnitude less than $S_\sigma(f=f_s)$. The best-fit line $S^c_\sigma(f)$ is obtained using the least-squares error method and the $N_\sigma(f_s)$ value is given by $N_\sigma(f_s)=S^c_\sigma(f=f_s)$.

The R plot exhibits a nonlinear dependence with σ. At $A_s=0.192B\approx 0.0029$, UWN dithering produces an R_{peak} value of 145.80 at $\sigma=\sigma_w\approx 0.004$. At $A_s=0.32B$, the peak value is 177.20 and is found at $\sigma=\sigma_w\approx 0.005$. At $A_s=0.96B$, it becomes equal to 180.81 and occurs at $\sigma=\sigma_w\approx 0.012$.

At $A_s=0.192B$, GN dithering produces an R_{peak} value of 173.34 at $\sigma=\sigma_g\approx 0.001$. At $A_s=0.32B$, $R_{\text{peak}}=203.0337$ and it occurs at $\sigma=\sigma_g\approx 0.002$. At $A_s=0.96B$, $R_{\text{peak}}=172.39$ and it occurs at $\sigma=\sigma_g\approx 0.008$. For both types of noise, the R vs σ profile broadens with increasing A_s value.

Our numerical results with dc thresholding indicate that dependence of R_{peak} on A_s does not have a wide dynamic range. With UWN dithering, the increase in the R_{peak} from $A_s=0.32B$ to $0.96B$ is only about 2%. With SC sampling, the corresponding increase is about 300% (see Fig. 5).

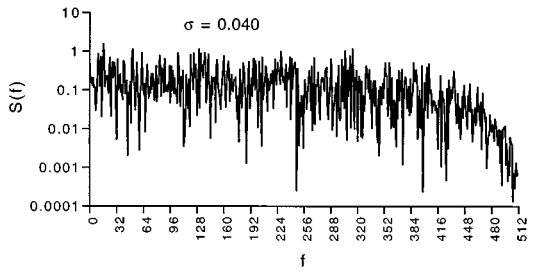

FIG. 11. Power spectrum $\{S_\sigma(f)\}$ produced when $s(t)=0.0029\cos(2\pi 16t)$ is dithered with UWN at $\sigma=0.04$, where $r(t)=2.5\cos(2\pi 512t)$, $B=0.015\,339\,8$, $T=1$, $2M=1024$, and $N=256$. The correct frequency of $s(t)$ is very difficult to ascertain from $\{S_\sigma(f)\}$. The plot illustrates that dithering becomes ineffective when σ values which are greater than σ_w are used.

The characteristics of the R vs σ plots produced with SC sampling (see Fig. 4) are distinctly different from those obtained using dc threshold sampling (see Fig. 10) because different criteria are used to define a crossing location, and to compute the autocorrelation function.

In SC sampling, a crossing t_i satisfies the relation $s(t)-r(t)=0$, where $r(t)$ is a sinusoid function. The autocorrelation $\gamma(kT/2M)$ is calculated from the interpolated (equally sampled and multivalued) amplitude representation $\{[s(iT/2M)+n_\sigma(iT/2M)]\}$ of $[s(t)+n_\sigma(t)]$. The procedure permits $\gamma(kT/2M)$ to contain information not only about the f_s value of $s(t)$ but also regarding its amplitude A_s.

On the other hand, any dc crossing t^{dc}_i satisfies the relation $s(t)\pm B=0$. The autocorrelation $\gamma_{\text{dc}}(kT/2M)$ is computed directly from the pulse sequence that is generated from the dc crossings of $s(t)+n_\sigma(t)$ with respect to $r(t)=\pm B$. The sequence can only have three possible values: 1, 0, and -1.

V. DISCUSSION

A. Quality of power spectrum

Our numerical experiments with $r(t)=2.5\cos(2\pi 512t)$ where $B=0.015\,339\,8$ show that the computed $\{S_\sigma(f)\}$ of $[A_s\cos(2\pi f_s t)+n_\sigma(t)]$ where $A_s<B$ exhibits only one prominent line which always occurs at $f=f_s$, if the σ value used corresponds to where the R plot is maximum. The frequency of the subthreshold oscillation $s(t)$ can therefore be established correctly and easily from $\{S_\sigma(f)\}$ when dithering is done at a noise variance that yields the peak R value. This behavior was found to be always true for $f_s<450\approx 0.88f_r$.

However, when stronger noise variances ($\sigma>\sigma_w$) are utilized to dither $s(t)$, the resulting $\{S_\sigma(f)\}$'s contain several prominent spectral lines at f values other than the one at $f=f_s$. The correct f_s value is very difficult to determine from such kinds of spectra.

Shown in Fig. 11 is the spectrum $\{S_\sigma(f)\}$ that is obtained when $s(t)=0.0029\cos(2\pi 16t)$ is dithered with UWN at $\sigma=0.040$. The frequency of $s(t)$ cannot be determined from the $\{S_\sigma(f)\}$ because (1) it exhibits many other distinct lines other than the one found at the true f_s value, and (2) the corresponding R of the $S_\sigma(f=16)$ line is low at $R\approx 5$.

Note in Fig. 4(a) that the R achieves a maximum value of about 345, at $\sigma_w\approx 0.017$. The appearance of the spurious spectral lines is due to false triggerings which become more

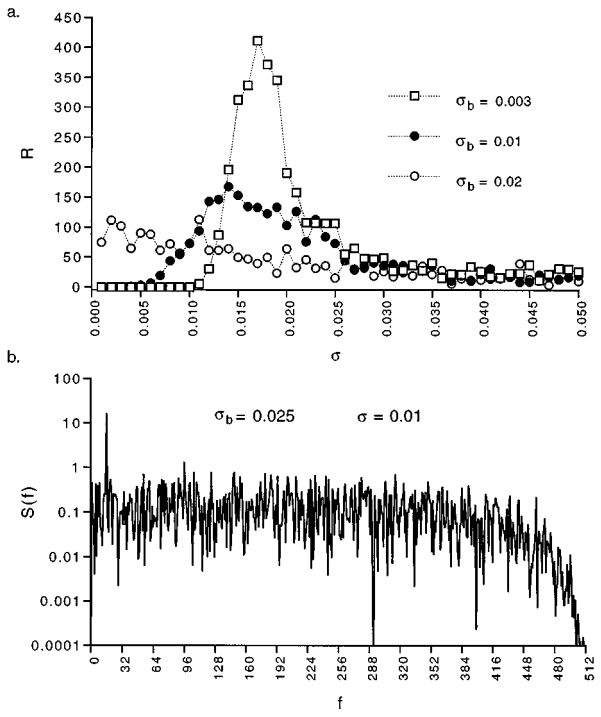

FIG. 12. Dithering and the presence of ambient noise $n_b(t;\sigma_b)$ where $r(t)=2.5\cos(2\pi 512t)$, $B=0.015\,339\,8$, $T=1$, $2M=1024$, and $N=256$. (a) R vs σ plots when $0.0029\cos(2\pi 16t)+n_b(t;\sigma_b)$ is dithered with UWN, (b) $\{S_\sigma(f)\}$ obtained at $\sigma=0.005$. Three different variances of $n_b(t;\sigma_b)$ are considered: $\sigma_b=0.003$, 0.01, and 0.025.

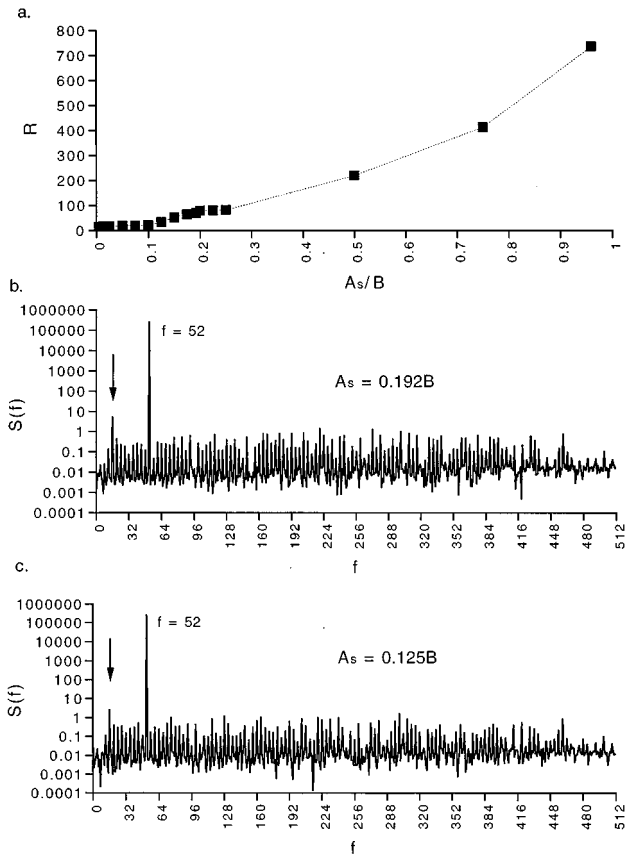

FIG. 13. Detection of subthreshold oscillation $s(t)=A_s\cos(2\pi 16t)$ by the addition of $s'(t)=1.0\cos(2\pi 52t)$, where $A_s<B=0.015\,339\,8$, $r(t)=2.5\cos(2\pi 512t)$, $T=2M\Delta=1$, $f_r=1/2\Delta=512$, $N=256$: (a) R vs A_s plot, (b) power spectrum of $s_2(t)=0.192B\cos(2\pi 16t)+1.0\cos(2\pi 52t)$, and (c) power spectrum of $s_2(t)=0.125B\cos(2\pi 16t)+1.0\cos(2\pi 52t)$. Without $s'(t)$, the R value of the $S(f=16)$ component is zero since $A_s<B$.

likely in each sampling interval Δ with increasing strength of the dither noise.

B. Dithering in the presence of ambient noise

We now consider the case when ambient white noise $n_b(t;\sigma_b)$ is also present at the input of the SC detector. This implies that prior to dithering, the signal that is at the detector input is $0.0029\cos(2\pi 16t)+n_b(t;\sigma_b)$. When the ambient noise is significant, preamplification is often ineffective in making $s(t)=0.0029\cos(2\pi 16t)$, detectable by the SC detector.

Figure 12(a) presents the R vs σ plots obtained when $0.0029\cos(2\pi 16t)+n_b(t;\sigma_b)$ is dithered with UWN. Three different strengths of $n_b(t;\sigma_b)$ are considered: $\sigma_b=0.003$, 0.01, and 0.025. Note that even at $\sigma_b=0.003$ it is already possible for ambient noise to have amplitude values which are already comparable to $s(t)$.

The R plots still exhibit the nonlinear behavior with σ especially for plots corresponding to $\sigma_b=0.003$ and 0.01. Notice, however, that R_{peak} decreases with increasing ambient noise. The peak location is also shifted to lower σ values of the UWN dither with increasing strength of the ambient noise. In the absence of ambient noise, the peak of the SNR curve occurs at $\sigma=\sigma_w\approx 0.017$ [see Fig. 4(a)]. The R plot also broadens with increasing ambient noise strength.

The $\{S_\sigma(f)\}$'s corresponding to the peak values of the R plots presented in Fig. 12(a) exhibit only one prominent line at $f=16$. Shown in Fig. 12(b) is the $\{S_\sigma(f)\}$ that is obtained when $0.0029\cos(2\pi 16t)+n_b(t;\sigma_b=0.025)$ is dithered with UWN at $\sigma=0.005$. The results in Figs. 12(a) and 12(b) indicate that the dithering technique remains effective even in the presence of strong ambient noise.

C. Addition of an above-threshold oscillation

In Sec. II we have seen that the quantization error E associated with a real SC detector is minimized for large amplitude values of the input signal because $E(p_i)=B|\sin(\pi p_i/N)|$, where p_i is the location within the interval Δ_i, when $x(t)=r(t)$.

We now examine whether a subthreshold oscillation $s(t)=A_s\cos(2\pi f_s t)$, where $A_s<B$, can be rendered detectable to the SC detector if it is added to a detectable oscillation $s'(t)=A_s'\cos(2\pi f_s' t)$, where $A_s'>B$.

Figure 13(a) illustrates how the R value of $S(f=f_s=16)$ in the power spectrum obtained from $s_2(t)$ changes with the A_s value where $s_2(t)=s(t)+s'(t)=A_s\cos(2\pi 16t)+1.0\cos(2\pi 52t)$, where $r(t)=2.5\cos(2\pi 512t)$, $T=2M\Delta=1$, $f_r=1/2\Delta=512$, $N=256$, and $B=0.015\,339\,8$. The power spectrum is given by the Fourier transform of the autocorrelation of $\{t_i''\}$ which are the solutions to $s_2(t)=r(t)$.

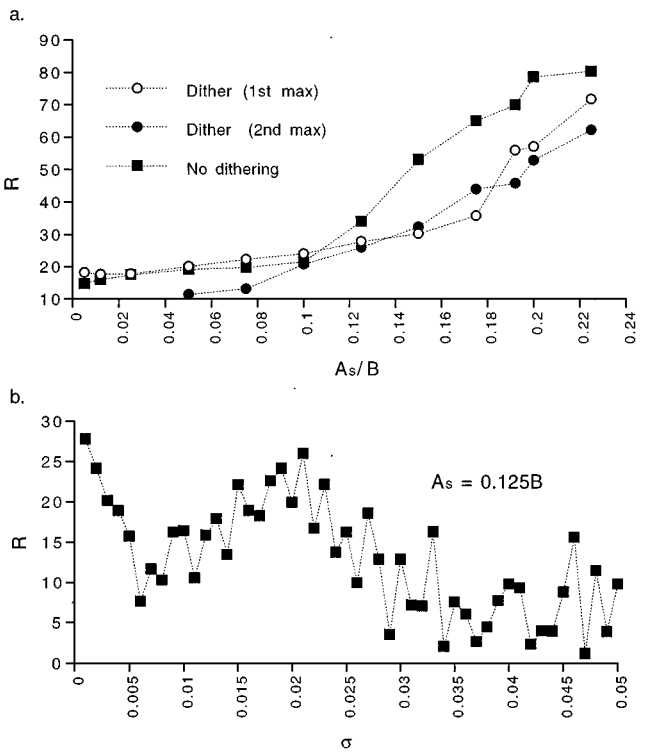

FIG. 14. Application of UWN dithering to $s_2(t) = A_s \cos(2\pi 16t) + 1.0 \cos(2\pi 52t)$, when $A_s \leqslant 0.24B$: (a) R vs A_s plots, (b) R plot from $[s_2(t) + n_\sigma(t)]$ where $A_s = 0.125B$. Parameters used: $B = 0.015\,339\,8$, $r(t) = 2.5 \cos(2\pi 512t)$, $T = 2M\Delta = 1$, $f_r = 1/2\Delta = 512$, and $N = 256$.

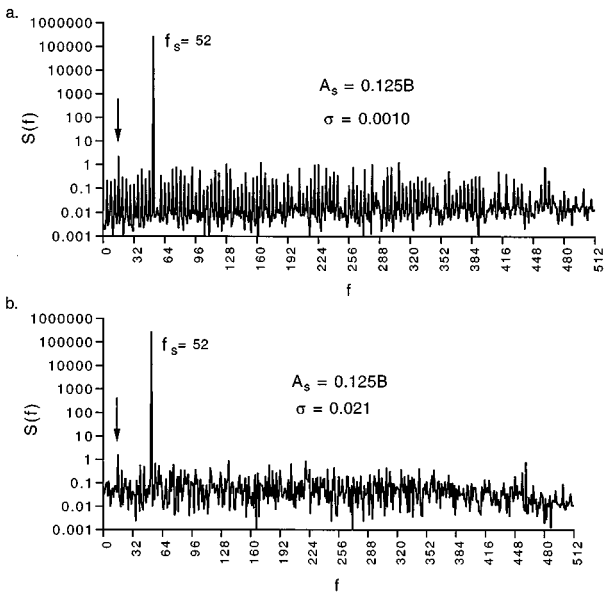

FIG. 15. Application of UWN dithering to $s_2(t) = 0.125B \cos(2\pi 16t) + 1.0 \cos(2\pi 52t)$, where $B = 0.015\,339\,8$, $r(t) = 2.5 \cos(2\pi 512t)$, $T = 2M\Delta = 1$, $f_r = 1/2\Delta = 512$, and $N = 256$: (a) $\{S_\sigma(f)\}$ produced at $\sigma = 0.0010$, and (b) $\{S_\sigma(f)\}$ produced at $\sigma = 0.021$.

The addition of $s'(t)$ to $s(t)$ improves the R value of $S(f=16)$ for all A_s values $< B$. Without $s'(t)$, R is zero because $A_s < B$. Presented in Fig. 13(b) is the corresponding power spectrum obtained for $A_s = 0.25B$, which clearly shows a distinct line at $f = 16$ (arrow). The component is the next strongest after the one at $f = 52$. The $S(f)$ components at frequencies other than $f = 16$ and 52 are not zero due to quantization errors.

Shown in Fig. 13(c) is the corresponding $\{S(f)\}$ obtained for $A_s = 0.125B$. It can be observed that the $S(f=16)$ line is already comparable in strength to the other spurious spectral lines caused by quantization errors. Adding a strong oscillation $s'(t)$ is no longer effective in detecting the frequency of the subthreshold oscillation $s(t)$ for $A_s \leqslant 0.125B$.

The (first) intersection between $r(t) = 2.5 \cos(2\pi 512t)$ and $s'(t) = 1.0 \cos(2\pi 52t)$, occurs at $p_i = 95$, when $T = 1$, $2M = 1024$, and $N = 256$. Thus the smallest quantization error is $E^{\min} = B|\sin(\pi p_i/N)| \approx B|\sin(\pi 95/N)| \approx 0.73B = 0.012$. By determining the f_s value from the power spectrum of the autocorrelation of $\{t_i''\}$, the frequencies of oscillations with amplitudes that are as low as $0.15B$ can still be determined without ambiguity. We now examine if dithering the composite signal $s_2(t) = s(t) + 1.0 \cos(2\pi 52t)$ is effective in determining the frequency of $s(t) = A_s \cos(2\pi 16t)$, in the case when $A_s \leqslant 0.125B$.

Figure 14(a) presents the R_{peak} vs A_s plots obtained from $s_2(t)$ when it is dithered with UWN. The results indicate that dithering decreases SNR decrease of the $S(f=16)$ component of $\{S_\sigma(f)\}$. For $A_s \geqslant 0.05B$, the R vs σ plots feature two possible peak values (first peak, open circle; second peak, solid circle).

Figure 14(b) presents the R plot of the $f = 16$ spectral component for $A_s = 0.125B$. The R plot exhibits a nonlinear dependence with σ. It has two maximum values—one at $\sigma = 0.001$ and another near $\sigma \approx 0.021$. It can be seen that the addition of noise to $s_2(t)$ initially decreases the R value until $\sigma \approx 0.006$, after which an increase is obtained that peaks at around $\sigma \approx 0.021$.

Figures 15(a) and 15(b) compare the $\{S_\sigma(f)\}$'s that are obtained when $s_2(t)$ is dithered with UWN at $\sigma = 0.001$, and $\sigma = 0.021$, respectively. It can be seen that dithering could not make the value of the $f = 16$ line more significant than the other spurious spectral components in $\{S_\sigma(f)\}$. Note further that dithering at $\sigma = 0.021$ produces an $\{S_\sigma(f)\}$ with weaker spurious components than the one obtained at $\sigma = 0.001$.

Recall that the dithering technique when implemented without the introduction of the strong oscillation is capable of determining unambiguously the correct frequency of $s(t)$ even for A_s values that are as low as $0.1B$. It also produces larger R_{peak} values (see Sec. IV C and Fig. 5).

D. Frequency- and amplitude-response characteristics

Figures 6(c) and 7(c) present the f_s-response characteristics of our detection technique. For both UWN and GN, the standard deviation of the $R_{\text{peak}}(f_s)$ values is less than 10% within the range $f_s \leqslant 384 \approx 0.75 f_r$. The f_s range where the dithering technique is effective can be expressed in terms of f_r so that the frequency f_s of any rapid subthreshold oscillation can be determined unambiguously by using a faster reference frequency $f_r > f_s/0.75$.

Within the range $0.1B \leqslant A_s \leqslant 0.9B$ our detection technique also produces a power-law relation between the R_{peak} value with the amplitude A_s of $s(t)$. The plots in Fig. 5 can be

used as calibration curves to determine the unknown A_s value from the measured R_{peak} value.

VI. CONCLUSION

This paper demonstrates a new dithering technique for improving the detection limit of a real SC detector. The technique is evaluated using benchmarks employed to investigate the nonlinear phenomenon of stochastic resonance.

The periodicity of the subthreshold oscillation $s(t)$ is rendered easier to detect by a cooperative effect in which a matching between the characteristic time scale of $s(t)$ which is a coherent signal, and that of the stochastic noise (with a broadband power spectrum) is induced with the result that the presence of the periodic component is greatly enhanced.

SC sampling is a nonlinear process because the locations $\{t_i\}$ where an input analog signal $x(t)$ intersects a reference sinusoid $r(t)$, does not obey the linearity property. This means that the solutions to $[x(t)+x'(t)]=r(t)$ are not given by $\{t_i+t_i'\}$ where $\{t_i\}$ and $\{t_i'\}$ are solutions to $x(t)=r(t)$, and $x'(t)=r(t)$, respectively. It is easy to see that the sampled representation produced by amplitude sampling at equal intervals of t obeys the linearity property.

The technique is effective if the dithered oscillation produces a power spectrum that exhibits only one prominent spectral line at $f=f_s$. This condition is guaranteed when the noise variance used in the dithering corresponds to the value that yields the maximum R for the $f=f_s$ spectral component.

Aside from determining the correct frequency of the subthreshold oscillation, our technique also gives a good approximation regarding the oscillation amplitude. However, it is incapable of determining the phase of the subthreshold oscillation because the power spectrum does not contain any information about it. We considered only uniform white-noise and Gaussian noise in the dithering experiments because they are among the simplest to generate [11]. A recent report, however, shows the stochastic resonance also occurs in chaotic systems [16].

Present work is confined to subthreshold oscillations. Experiments are on-going to extend the technique to weak multifrequency signals. A comprehensive theoretical treatment which can explain our results more quantitatively is also beyond the scope of the present study. The results that we have obtained indicate the theory that has been previously developed to describe dithering in dc threshold sampling [9] is insufficient.

ACKNOWLEDGMENTS

The authors thank May Lim for her assistance in the computation of the signal-to-noise ratio plots. This work was supported by the National Research Council of the Philippines.

[1] C. Blanca, V. Daria, and C. Saloma, Appl. Opt. **35**, 6417 (1996).
[2] C. Saloma, Phys. Rev. E **53**, 1964 (1996).
[3] V. Daria and C. Saloma, Rev. Sci. Instrum. **68**, 240 (1997).
[4] C. Saloma and V. Daria, Opt. Lett. **18**, 1468 (1993).
[5] A. Longtin and K. Hinzer, Neural Comput. **8**, 215 (1996).
[6] J. Maunsell, Science **270**, 764 (1995).
[7] J. Hopfield, Nature (London) **376**, 33 (1995).
[8] W. Bennet, Bell Syst. Tech. J. **27**, 446 (1948); A. Oppenheim and R. Schaffer, *Digital Signal Processing* (Prentice-Hall, New York, 1975).
[9] L. Gammaitoni, Phys. Rev. E **52**, 4691 (1995).
[10] K. Wiesenfeld and F. Moss, Nature (London) **373**, 33 (1995); A. Bulsara and L. Gammaitoni, Phys. Today **39**, 3 (1996); J. Douglass, L. Wilkens, E. Pantazelou, and F. Moss, Nature (London) **365**, 337 (1993); H. Braun, H. Wissing, K. Schafer, and M. Hirsch, *ibid.* **367**, 270 (1994); J. Levin and J. Miller, *ibid.* **380**, 165 (1996); M. Inchiosa and A. Bulsara, Phys. Rev. E **53**, R2021 (1996); S. Bezrukov and I. Vodyanoy, Nature (London) **385**, 319 (1997); E. Reibold, W. Just, J. Becker, and H. Benner, Phys. Rev. Lett. **78**, 3101 (1997).
[11] G. E. Johnson, Proc. IEEE **82**, 270 (1994).
[12] C. Saloma and M. Escobido, Appl. Opt. **33**, 7617 (1994).
[13] W. Press, B. Flannery, S. Teukolsky, and W. Vetterling, *Numerical Recipes* (Cambridge University Press, Cambridge, England, 1986).
[14] J. Proakis and D. Manolakis, *Digital Signal Processing: Principles, Algorithms and Applications*, 2nd ed. (Macmillan, New York, 1992), pp. 943 and 944.
[15] P. deVries, *A First Course in Computational Physics* (Wiley, New York, 1994).
[16] E. Reibold, W. Just, J. Becker, and H. Benner, Phys. Rev. Lett. **78**, 3101 (1997).